Is geometry more universal than physics in atmospheric boundary layer flow?

D. Belušić[1] and L. Mahrt[2]

Received 5 October 2011; revised 30 March 2012; accepted 6 April 2012; published 10 May 2012.

[1] We show that the geometry of motions in atmospheric boundary-layer time series exhibits considerable independence from scale in spite of changing physics. The scale-independence of structure shapes is shown by using a simple technique to extract basic shapes from the time series for timescales between 3 s and 2 h. A set of predefined basic shapes is chosen subjectively as those that occur most frequently in the time series: sine, step, ramp-cliff and cliff-ramp. The frequency of occurrence of shapes changes with the timescale, with a pronounced minimum at scales between 2 and 10 min depending on the stability and the shape function. This is in accordance with the minimum of kinetic energy between turbulence and mesoscales. However, the ratios of occurrences between different shapes are approximately scale-independent. What shapes are preferred depends only on the variable examined. The physics of different shapes and scales is examined from characteristics of individual shapes. Steep edges of shapes seem to be predominantly related to downward transport of heat and momentum, which weakens with increasing scale. Sine shapes on the other hand seem to be related to turbulent eddies and shear instability at small scales, and to internal gravity waves at larger scales with stable stratification. Therefore, the physics of individual shapes is shown to change with scale, while the geometry seems to remain approximately scale-independent.

Citation: Belušić, D., and L. Mahrt (2012), Is geometry more universal than physics in atmospheric boundary layer flow?, *J. Geophys. Res.*, *117*, D09115, doi:10.1029/2011JD016987.

1. Introduction

[2] Basic shapes of coherent structures in turbulent flows frequently include sharp edges or zones of semi-discontinuities [e.g., *Hunt et al.*, 2010] as often viewed in terms of ramp-cliff structures of passive scalars [*Wilczak*, 1984; *Warhaft*, 2000; *Shraiman and Siggia*, 2000] and microfronts [e.g., *Mahrt*, 1991]. These features were reported as early as *Taylor* [1958] for temperature in the atmospheric boundary layer (ABL) and attributed to convective plumes. Later laboratory and numerical studies showed that these structures can occur irrespective of the sign of thermal stability [e.g., *Mestayer et al.*, 1976; *Gibson et al.*, 1977; *Warhaft*, 2000, and references therein], without the presence of a boundary [e.g., *Gibson et al.*, 1977; *Wroblewski et al.*, 2007], and even appear in two-dimensional random Gaussian velocity fields [*Holzer and Siggia*, 1994]. *Shraiman and Siggia* [2000] and others therefore suggest that the statistics of the scalar turbulence can be decoupled from the underlying velocity field, and as such the scalar intermittency, defined as the departure from a gaussian distribution with the excess of large bursts at smaller scales, is inherent to the mixing process itself. Due to these characteristics, the scalar turbulence yielded to a simpler theoretical approach [*Shraiman and Siggia*, 2000]. However, it seems that the structure of turbulent velocity fluctuations is less amenable to such a treatment.

[3] Events or coherent structures, such as ramp-cliff patterns discussed above, appear to dominate atmospheric turbulent flows in canopies due to the canopy-induced inflection point instability [e.g., *Finnigan*, 2000]. It has recently been proposed that these events render the flow "more deterministic", in a sense that their presence reduces the embedding dimensions of underlying phase space attractors [e.g., *Campanharo et al.*, 2008]. In this manner, the otherwise highly complex atmospheric turbulent flows start behaving as lower-dimensional less chaotic systems [e.g., *Wesson et al.*, 2003]. In addition, there are many different physical processes in the atmosphere, often of abrupt nature, that force, modify and coexist with the turbulence over a broad range of scales [e.g., *Belušić and Mahrt*, 2008], including atmospheric gravity waves, thermally induced mesoscale flows and so forth. Therefore, the event-like features are ubiquitous in the atmosphere at all scales and significantly contribute to flow properties, such as transport of scalars and generation of smaller scale turbulence [e.g., *Sun et al.*, 2004; *Vindel and Yagüe*, 2011].

[4] The range of scales just larger than the three-dimensional turbulence, sometimes termed submesoscales,

[1]Monash Weather and Climate, School of Mathematical Sciences, Monash University, Clayton, Victoria, Australia.
[2]COAS, Oregon State University, Corvallis, Oregon, USA.

Corresponding author: D. Belušić, Monash Weather and Climate, School of Mathematical Sciences, Monash University, Clayton, VIC 3800, Australia. (danijel.belusic@monash.edu)

0148-0227/12/2011JD016987

appears to be the least understood aspect of the ABL, particularly in the weak-wind stable ABL. There the flow is evidently composed of events with a wide range of amplitudes [e.g., *Mahrt*, 2011]. While large-amplitude well defined events are more often examined [e.g., *Sun et al.*, 2002; *Viana et al.*, 2009], the results are not easily extendable to common weaker events. Therefore, the origin and nature of these motions is at this point unknown. The most probable scenario is that we are witnessing a melange of gravity waves, drainage flows, shear instabilities, solitons and other more complex modes.

[5] Simple visual inspections of various ABL time series reveal that common shapes appear on a large range of timescales, from the smallest turbulence scales up to tens of hours. These shapes may be of any amplitude, but are of surprisingly similar geometries across the scales in spite of substantial change of physics with scale. This provokes another question: Is it possible to distinguish between different scales, having time series with equal number of points, but not knowing the sampling rate? An answer is indicated in randomly chosen examples in Figure 1, where an untrained eye cannot distinguish between the shapes on different scales.

[6] The purpose of this study is to examine the dependence of different flow geometries on stability and timescale, as well as document structural shapes and their orientations in the time series. Usually, the quest for coherent structures is limited to some expected timescales (such as 1 min) and to large amplitudes [e.g., *Gao et al.*, 1989; *Krusche and De Oliveira*, 2004; *Barthlott et al.*, 2007]. In this study, we apply neither restriction. In contrast to previous studies, we allow a very large range of timescales, here between 3 s and 2 h. The large-amplitude limit is relaxed by not using variance-based methods, but instead simple linear correlation (section 2). This study is intended as a preliminary survey in order to gain information and determine future avenues for in-depth analyses.

2. Data and Methods

2.1. Data

[7] An eddy correlation tower located in Kutina, Croatia (45.476N, 16.796E) was equipped with 7 levels of Gill Windmaster and Windmaster Pro sonic anemometers. It was located in a relatively small (480 m $\times$ 120 m) mixed forest, approximately 20 m high, with a complex direction-dependent footprint including urban and suburban areas, a large factory, open fields and small hills. Kutina is in a broad valley surrounded by complex terrain. A mountain ridge about 10 km to the north of Kutina is about 500 m high. There were five sonics above the canopy height, and here we use only the sonic at 40 m above ground level. The sonic wind and temperature were recorded at 20 Hz sampling frequency. The measurements were performed from 17 September 2008 to 18 October 2009. Data were quality checked both manually and using an improved version of *Vickers and Mahrt* [1997]. No tilt correction was applied, because the shape-searching analysis in this study is performed only on the temperature and horizontal wind speed. The vertical velocity is used to complement the information on the dynamics of different shapes, and it is considered only relative to its mean, i.e. in terms of phase alignment with the temperature and horizontal wind speed. In that sense, the mean vertical velocities do not impact the analysis.

2.2. Method

[8] The goal is to recognize different structural shapes from the time series of the wind speed and the temperature. The geometries of the shapes were subjectively chosen as the most basic shapes after consulting the time series. These are: a simple sine function, a step function, a ramp-cliff function, and a cliff-ramp function (or a reversed ramp-cliff); see Figure 2. These basic shapes may correspond to certain physical features in the atmospheric boundary layer: a wave (sine), a (micro)front (step) [e.g., *Mahrt*, 2010a], and differently oriented turbulent ramp-cliff patterns [e.g., *Antonia et al.*, 1979]. This paper differs from conditional sampling studies in that we employ a variety of the most basic shapes to describe the entire record, rather than choosing one shape to study a particular structure (for example, using the step function or ramp functions to study thermals in a sheared environment).

[9] The method for shape recognition is based on the linear correlation between a theoretical shape and the time series as viewed in terms of a moving window of various scales. The linear correlation is chosen because it is based on the geometry of a shape more than on its amplitude. All other methods involving multiplication [e.g., *Mahrt*, 2010a] or convolution (all power spectral methods, including wavelet and Fourier analysis) favor large-amplitude events. While the latter approach has many advantages, one of them being that the most energetic features are usually the most important ones in terms of fluxes, it reduces the importance of the exact shape of the feature. The shapes across different scales tend to have very similar geometries, but significantly different amplitudes. Therefore, the linear correlation will ensure that primarily shapes with similar geometries will be extracted. The correlation will nominally take into account the amplitude of a given feature, because its amplitude has to be larger than the surrounding "noise" on smaller timescales in order to be recognized. In that sense, the linear correlation will extract "clear" shapes of any strength that are embedded within a "less energetic" environment.

[10] Here the subjective criterion for shape recognition is based on the absolute correlation coefficient: $r > 0.9$. The relatively high value of 0.9 was chosen after several tests in order to most clearly distinguish between different shapes, although this choice significantly reduces the final sample size. The procedure is applied to a range of scales, from the smallest possible, given the data sampling rate, to the largest scale with sufficient sample size, limited by the length of the time series. A theoretical shape with an arbitrarily chosen width of 60 data points moves sequentially point-by-point through the time series and the correlation coefficient is calculated for each location. The time series are suitably averaged so that 60 data points define the timescale under consideration. Therefore, the sampling rate of 20 Hz enabled the minimum shape timescale of 3 s, with subsequent scales distributed as follows: 18 s, 1 min, 2 min, 5 min, 10 min, 20 min, 30 min, 1 h and 2 h. Scales larger than 2 h were eliminated due to inadequate sample size. The entire procedure required a large amount of computational time;

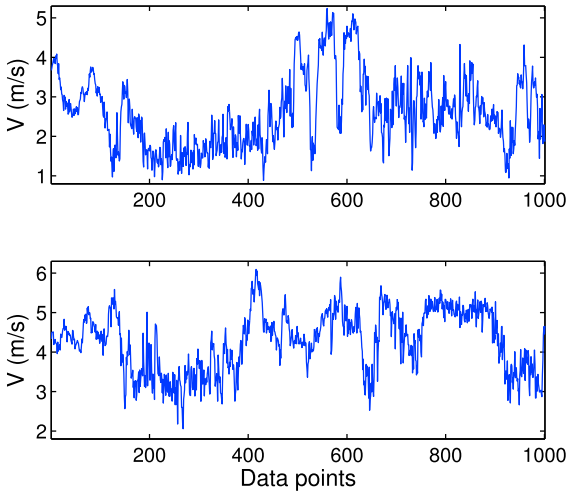

Figure 1. Wind speed time series with 1000 data points measured at the same location, given for two different sampling rates: (top) 60 s and (bottom) 0.05 s.

therefore the smallest two scales (3 and 18 s) were calculated over a subset of the data, namely over four months roughly spanning all seasons (January, April, July and September 2009). Each of the shapes can have two orientations with respect to the values of the variable, i.e. a shape can start with (or, as used here, its steeper part can have) either a positive or negative $\partial/\partial t$. Therefore, eight shapes are required for completeness (see Figure 2). In the shape searching algorithm, the first selected shape has the largest r for a specific timescale within the entire time series. After it has been categorized and selected, that part of the time series is excluded from further analysis in order to avoid overlaps of different shapes, and the shape with the next largest r is chosen. This procedure continues, for each timescale separately, until all shapes with $r > 0.9$ are selected. The following describes the progression of individual steps.

[11] 1. Sequentially advance a predefined shape function point-by-point through the entire time series, and calculate r at each point. Repeat the same procedure for all other predefined shape functions.

[12] 2. Save the properties (location, length, etc.) of the selected observed structure with the largest value of r, and then remove the corresponding part of the time series.

[13] 3. Select the shape with the next largest r. Continue until all shapes with $r > 0.9$ have been selected.

[14] 4. Reset the procedure. Block average the unmodified time series to a scale that is 60 times smaller than the next desired timescale of shapes. In our case, the next timescale of shapes is 18 s, so the raw data are averaged to 0.3 s.

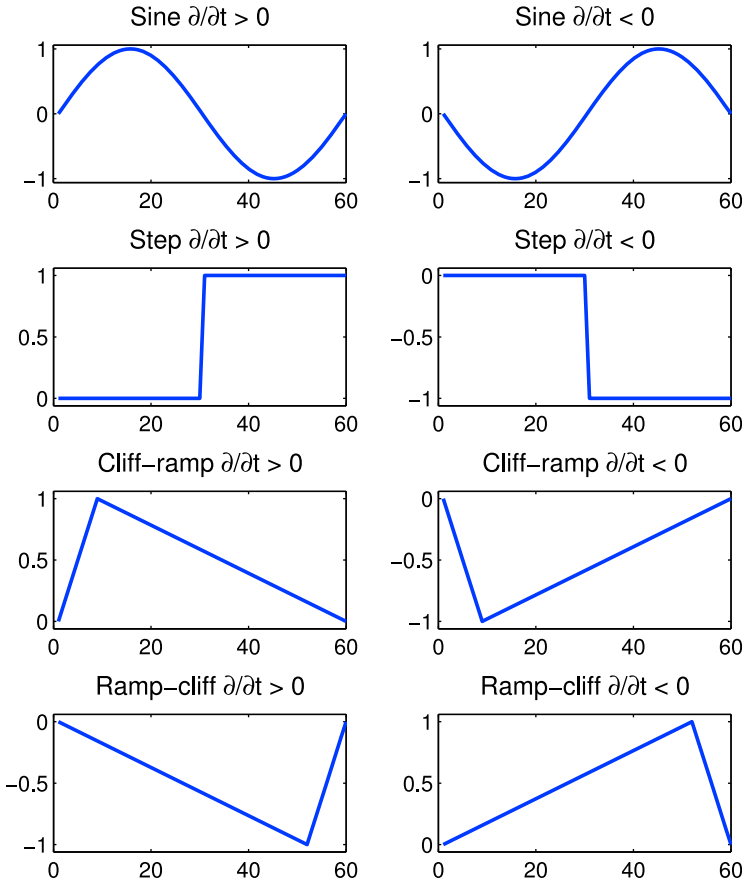

Figure 2. Shape functions used in this study: sine, step, cliff-ramp and ramp-cliff, with both orientations (positive or negative $\partial/\partial t$). The orientation is defined based on the steeper part of the shape, except for the sine function where the distinction is equivalent to a phase shift and is given only for completeness.

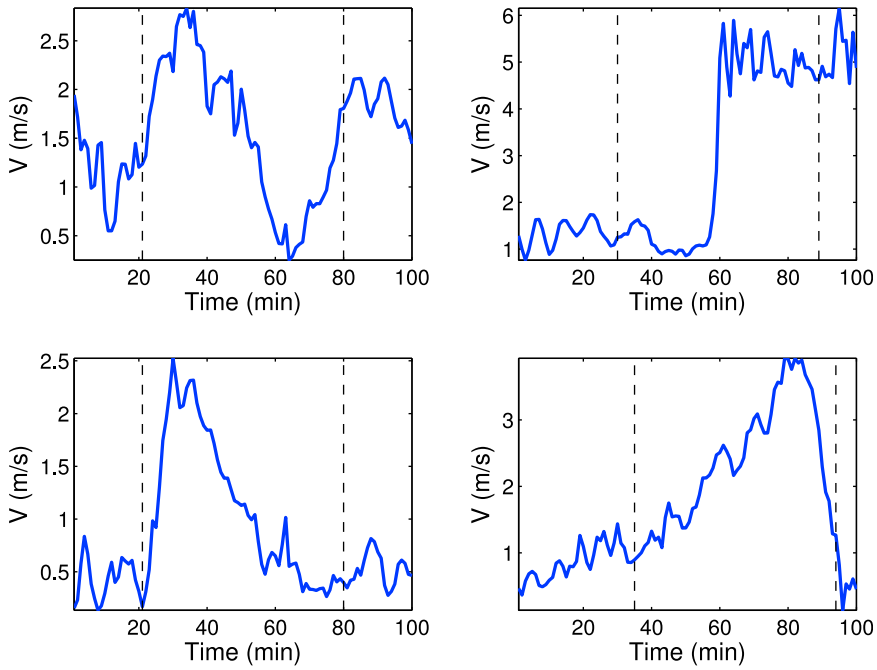

Figure 3. Examples of different 1-h shapes recognized from 1-min averaged wind speed time series. Black vertical dashed lines indicate the 60 points used for the recognition of the shape. Compare to Figure 2.

Repeat all previous steps. Continue in the same manner for all desired scales.

[15] The threshold criterion for the correlation coefficient was found to be insufficient for theoretical step shapes, and theoretical sine shapes when correlated with step-like shapes in the time series, because the correlation of step shapes with other shapes tends to be large even when other shapes have gradual changes, which is due to the discontinuity of the step function [e.g., *Anscombe*, 1973]. Therefore, additional criteria are used in order to verify the existence of the sudden step-related change. These additional criteria were subjectively determined from many observations of falsely recognized step and sine shapes. We require that the difference of medians of four data points before and after the shape center is smaller (greater) than 40% of the maximum absolute difference between any two points in the shape for theoretical sine (step) function. It should be noted that while providing visually somewhat better defined structures of recognized shapes, the overall effect of this procedure on the final results is minor due to a relatively small number of falsely recognized shapes in the first place. Due to the asymmetry, the ramp shapes do not require such criteria. Finally, this method essentially automatizes visual pattern recognition. Therefore, the verification of the method is trivial, although time consuming – a simple visual inspection of the captured structures [see, e.g., *Cava et al.*, 2004]. An additional test was performed on a limited portion of the time series, where the portion of the time series was phase randomized. The procedure includes taking the Fourier transform of the original signal, randomizing the phase while keeping the magnitude of the transform, and reverting back to the time domain using the inverse Fourier transform. Phase randomization should remove coherent structures from the time series, since they are primarily characterized by phase correlations [e.g., *Armi and Flament*, 1985]. The shape-searching method was then applied to both the original and phase-randomized portion of the time series. It recognized about 90% less shapes for phase-randomized data compared to the original data, which clearly shows that the method is not recognizing structures where they do not exist. Visual inspection confirmed that the shapes that were recognized by the method from phase-randomized data were actual structures present in the phase-randomized time series, implying that the phase-randomization did not remove all coherent structures from the time series.

3. Results and Discussion

[16] Examples of recognized shapes are shown in Figure 3. Similar structures appear for all the scales examined here. For example, the sine shape for the smallest scales usually appears only as a single wavelength embedded within a chaotic environment abundant in many other shapes. These are most probably not waves, but the signatures of small turbulent eddies. On the other hand, trains of sinusoidal shapes can be occasionally noticed for larger scales with stable conditions, suggesting gravity waves. Later discussion will show that for sine shapes, the phase angles between different variables change with the scale.

[17] Two main aspects of the shapes are examined: the dependence of the different geometries on the timescale, and the significant characteristics of different shapes. The latter reveals that different shapes and scales are associated with different physical mechanisms. The analysis is separated in two broad stability categories: unstable conditions ($z/L < -0.1$) and stable conditions ($z/L > 0.1$), where a single value of z/L characterizes an entire shape. Here z denotes the height of the measurements above the displacement height d,

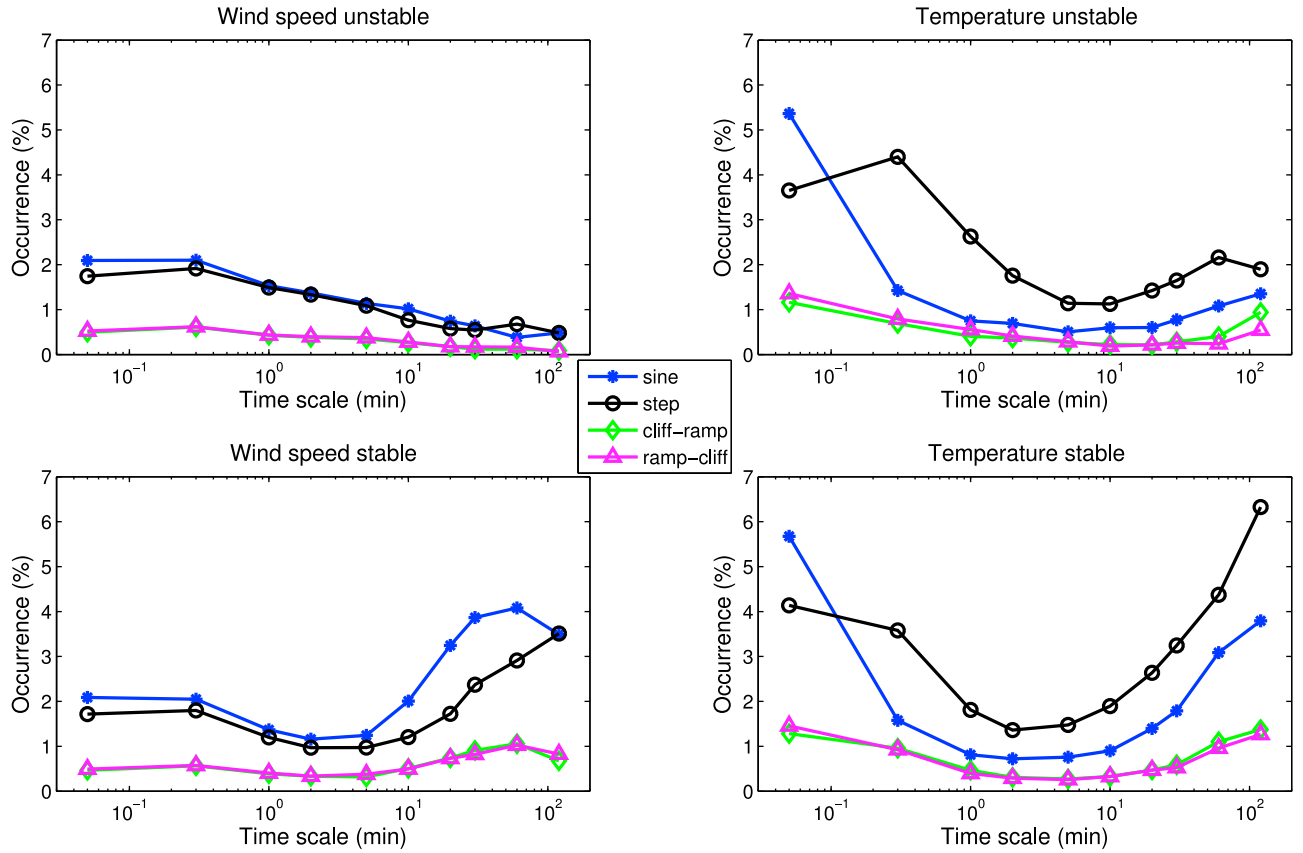

Figure 4. The number of recognized (left) wind speed and (right) temperature events relative to the theoretically maximal number of events for each scale for (top) unstable and (bottom) stable conditions.

where d is estimated as 2/3 of the canopy height yielding z = 27 m, and L is the Obukhov length:

$$L = -\frac{u_*^3 \overline{\theta}_v}{\kappa g \left(\overline{w'\theta'_v}\right)},$$

where u_* is the friction velocity, θ_v is the virtual potential temperature, w is the vertical wind speed, κ is the von Karman constant, g is the gravity acceleration, primes denote perturbations from 1-min averages, and overbars denote the time average over the length of the shape. A stability-dependent averaging time for defining perturbations might have been more appropriate [e.g., *Acevedo et al.*, 2006; *van den Kroonenberg and Bange*, 2007], but here, L is used only for broad classification of the data. The 1-min averaging time was chosen to minimize contamination of fluxes by mesoscale motions for stable conditions [e.g., *Basu et al.*, 2006; *Vickers and Mahrt*, 2006; *Viana et al.*, 2010]. Tests with using perturbations from 5-min averages showed negligible differences compared to the 1-min averages. The influence of anemometer tilt correction is not important for classification of the data. The stability categories are chosen to be broad to maximize the sample sizes for larger scales. As revealed from tests with narrower stability classes, the sensitivity to the choice of the threshold value of z/L is small.

3.1. Occurrences of Shapes

[18] The number of occurrences of recognized shapes is given in Figure 4 as the percentage of the theoretical maximum number of shapes for a certain scale and data period. The theoretical maximum is the ratio of record length to the window width, and hence does not depend on the geometry of the shape. The ratio of numbers of different recognized shapes for each scale shows whether different scales foster smoother, wave-like shapes or sharp, front- or ramp-like shapes.

[19] Figure 4 shows that the number of occurrences for temperature shapes under unstable conditions has a minimum at roughly 5 min for sine and step functions and at approximately 10 min for both ramp functions. It is likely that the ramp functions capture the entire asymmetric thermals whereas the step and sine functions capture the upwind sharp edge of the thermal and immediate environment. For temperature with stable conditions, the minimum is located at smaller timescales. Sine and step shapes have a minimum at 2 min, and ramps at 5 min. This behavior is consistent with the expectation that the scale of the turbulence is smaller for stable conditions compared to unstable conditions. As a working hypothesis, we assume that the motions on scales smaller than the minimum are turbulent while larger scales are nonturbulent motions on submeso/meso scales. That is, the minima in the number of occurrences could be related to the energy "gap" between the turbulence and submeso/mesoscales that is sometimes observed in the power spectra. The later gap is based on kinetic energy while the former shape gap is based on integrity of the structures (correlation). The presence of the gap with both types of scales dependencies suggests well organized turbulent

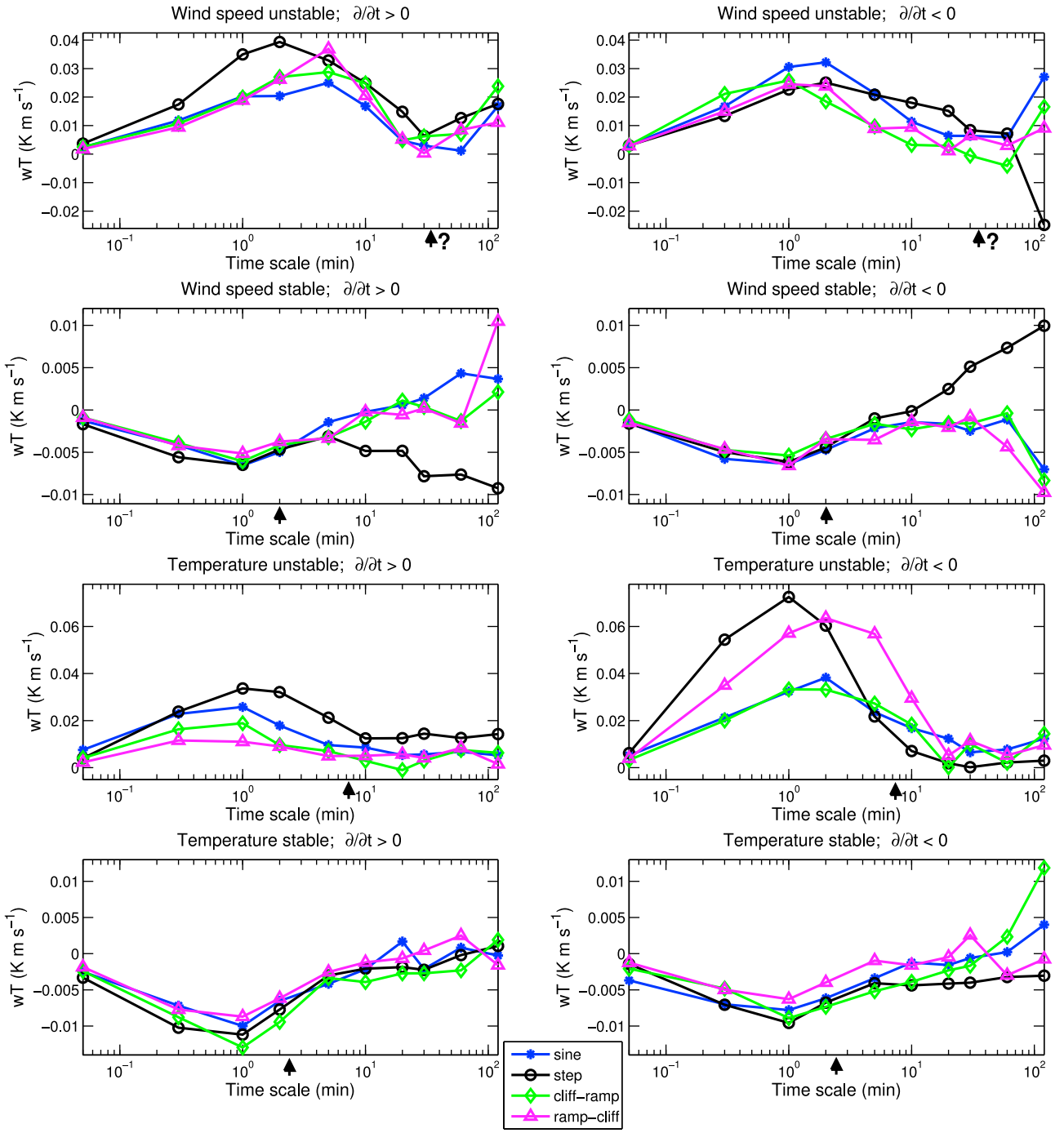

Figure 5. Scale dependent vertical heat flux for wind speed and temperature events, for unstable and stable conditions. Shapes with (left) positive and (right) negative $\partial/\partial t$ (see Figure 2) are contrasted. Vertical arrows indicate the approximate timescale of the minimum of occurrences (see Figure 4).

structures and well organized meso/submeso structures separated by the gap. For wind speed, the decrease of occurrences is extended over almost all scales for unstable conditions. Larger scale wind structures are evidently poorly organized in unstable conditions. Under stable conditions the occurrences have minimum at about 2 min (Figure 4). Large-scale motions in the unstable case show much less coherence of the wind field compared to the temperature field.

[20] For both temperature and wind speed, the increase of occurrences with increasing scale for scales greater than the occurrence minimum is much steeper for stable than for unstable conditions, particularly for sine and step shapes. As a result, large-scale coherent structures are substantially more common with stable stratification compared to unstable stratification. While our analysis does not take into account amplitudes of shapes, the application of several

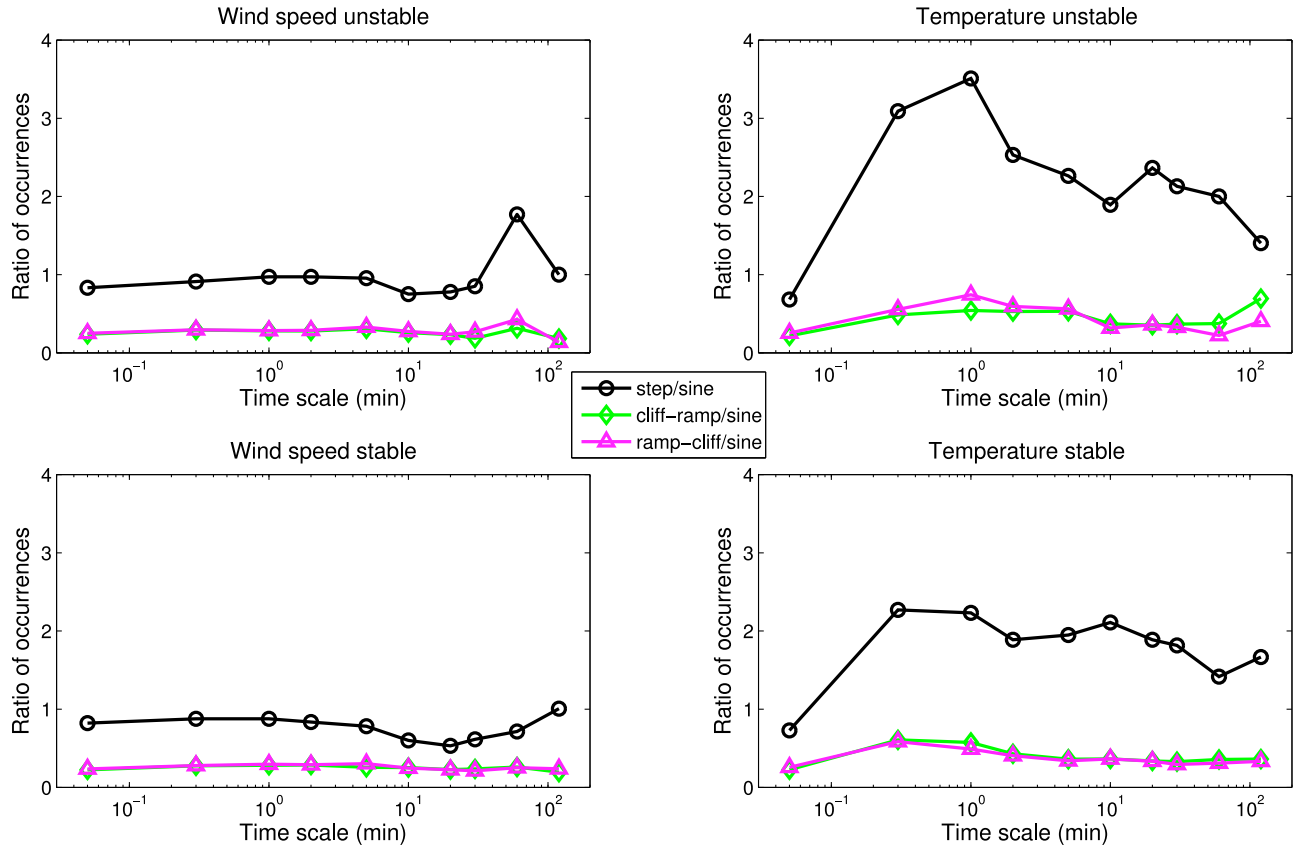

Figure 6. Ratio of numbers of different recognized (left) wind speed and (right) temperature events for each scale for (top) unstable and (bottom) stable conditions.

amplitude thresholds to both temperature and wind speed at larger scales did not yield significant differences to this finding. Presumably, the difference between stable and unstable shape occurrences is because the stratification leads to preference for horizontal growth of perturbations while unstable conditions promote vertical growth. However, to the best of our knowledge, studies that could confirm or reject this hypothesis do not exist in the literature.

[21] As an aside, the ramp-cliff shapes exhibit almost the same behavior as the cliff-ramp shapes, potentially implying a minor role of the expected asymmetric organization of the structures due to the shear [e.g., *Wilczak*, 1984]. However, the physics provides a different picture, as shown in the following.

[22] The transition between the turbulence and larger scales is usually identified from the vertical heat flux cospectra as either the scale where the heat flux falls below a threshold value or where it first crosses zero. Here we calculate the heat flux for each shape and scale from the 60 data points within each selected shape. The perturbations are calculated as deviations from the 60-point mean for each scale. The flux is thus not the total turbulent flux but rather the flux associated with only a certain shape and scale. These fluxes are averaged over all of the data for a given scale for each shape to provide the scale dependence of the heat flux for each shape, as depicted in Figure 5. The heat flux maxima tend to appear at larger timescales for unstable than for stable conditions, which is in accordance with the usual observations. The heat flux falls off at smaller scales for stable conditions, implying smaller "gap" scale for stable conditions. Figure 5 indicates that the increase of occurrences for larger times scales (Figure 4) does not lead to significant heat flux, consistent with the expectation of little flux for the mesoscale range.

[23] Distinguishing between the shapes with positive and negative $\partial/\partial t$ (see Figure 2 for the definition) reveals that certain shapes and orientations contribute to the heat flux more than others (Figure 5). For temperature shapes in unstable conditions, the step and ramp-cliff shapes with sudden temperature decrease ($\partial T/\partial t < 0$) dominate the flux for scales between 18 s and 5 min. This is consistent with asymmetric thermals subject to background wind shear, where the downwind diffuse part of the structure reaches the tower before the upwind steep part. The latter corresponds to the ramp-cliff or step with $\partial T/\partial t < 0$ in the time series. Thermals dominate the heat flux, as expected. Fluxes at larger timescales for stable conditions are generally considered to be unreliable, because the very weak vertical motions in those conditions are hard to measure (see references in *Mahrt* [2010b]).

[24] The apparent disagreement between the frequency of occurrence, where ramp-cliff and cliff-ramp shapes seem to be equally represented, and the heat flux, where ramp-cliff shapes with $\partial T/\partial t < 0$ dominate, is probably due to significant contribution to the heat flux by only a small number of ramp-cliff shapes, while the majority of other structures

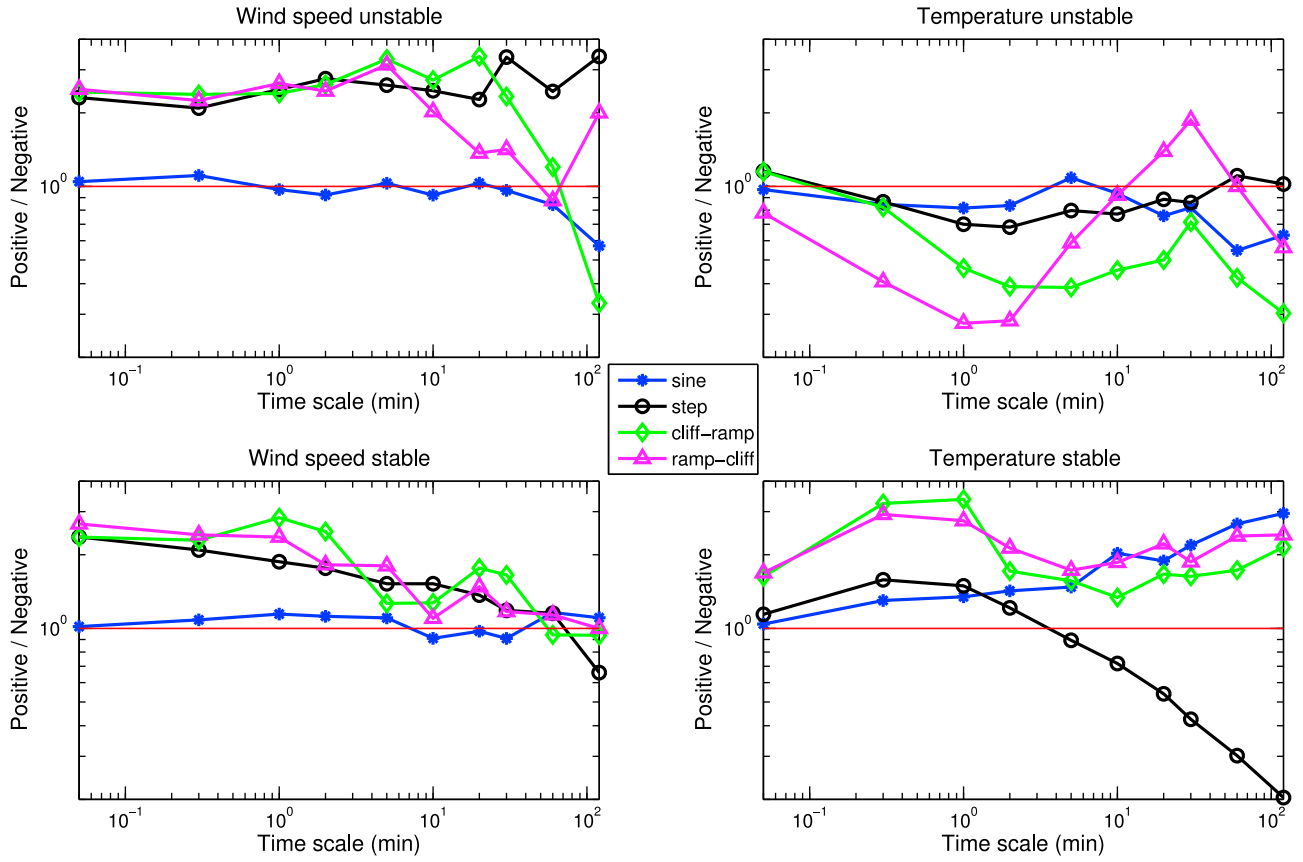

Figure 7. Ratio of number of shapes with positive $\partial/\partial t$ to number of shapes with negative $\partial/\partial t$ for each shape function. See also Figure 2.

transport less efficiently. These less-active shapes show no preference for the orientation of the cliff slope. Furthermore, the site heterogeneity may be responsible for modification of shapes and hence contribute to the above differences.

[25] The ratio of occurrences between different shapes is generally roughly independent of scale though it can be significantly different from unity (Figure 6). This is particularly visible for the ratio of ramps to sines, which is approximately constant for all conditions and scales, and tends to be 0.3 for the temperature and 0.2 for the wind speed. That is, sine patterns are more frequent than ramp patterns, but the ratio of frequency of occurrence does not depend on scale. This semi independence of scale survives the fact that the physics and vertical transport associated with these structures (Figure 5) do depend on scale. It may be that these fundamental shapes are so common that a similar result would be obtained for many other time series not even necessarily related to geophysical flows.

[26] The frequencies of the ramp-cliff and cliff-ramp shapes are similar (see also Figure 4). For temperature, there are more sharp front-like structures than smoother waves, except for the smallest scale. For wind speed, the sine shapes dominate all but the 1-h scale in unstable conditions. The relative sharpness of the temperature shapes compared to the wind shapes is probably due to pressure fluctuations and shear instability, which "act" to smooth out near discontinuities in the wind field.

3.2. Common Characteristics of Different Shapes

[27] For the majority of shapes and scales, the increase in wind speed V across the structure is related to a decrease in the vertical motion, w, across the structure (not shown). This behavior corresponds to negative correlation between w and V, and indicates downward momentum flux. However, w tends to weaken with increasing scale, so this relation becomes less clear with increasing scale. For stable conditions, w and T are on average 180° out of phase, while they are in phase for unstable conditions (e.g., rising warm air in thermals). Again, this relation weakens with increasing scale. These relationships are in accordance with the usual ABL observations and theory, as they essentially represent the downward momentum flux near the surface, and the downward (upward) heat flux in stable (unstable) conditions, and that the fluxes become small at the largest scales.

[28] For small and intermediate timescales, the sharp wind speed shapes (steps and cliffs) have predominantly positive $\partial V/\partial t$, i.e. their steep edges correspond to rapid increases of wind speed at the tower. Figure 7 indicates that there are more shapes whose steeper part corresponds to acceleration than those that are characterized by deceleration (negative time derivative). This behavior is consistent with frontogenesis on micro scales where horizontal convergence (speed increases) leads to sharper gradients compared to decreasing speed. That is, using Taylor's hypothesis, horizontal convergence ($\partial u/\partial x < 0$) corresponds to $\partial u/\partial t > 0$

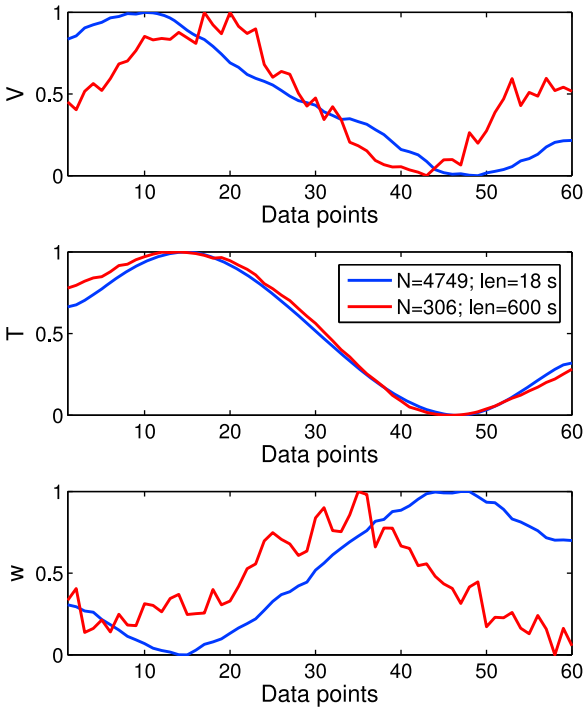

Figure 8. Sine shapes recognized from temperature time series with timescales 18 s (blue) and 10 min (red) under stable conditions, averaged over N records. (top) Wind speed (V), (middle) temperature (T) and (bottom) vertical velocity (w) are scaled as $\phi_{scaled} = \frac{\phi - \min(\phi)}{\max(\phi) - \min(\phi)}$, where ϕ stands for V, T or w.

observed at a fixed point. Similar tendency occurs for temperature shapes for stable conditions, while for unstable conditions the situation is reverse. Additionally, for almost all shapes, this tendency decreases or even reverses sign with increasing scale.

[29] The generation of sharp events by downward motions and mixing of higher momentum would explain both the systematic positive $\partial V/\partial t$, and the positive (negative) $\partial T/\partial t$ in stable (unstable) conditions. Furthermore, with increasing scale, the motions become more horizontal and two-dimensional, thus reducing the effect of downward flux and the associated tendencies in steep parts of the wind speed and temperature shapes. As expected, the sine shapes generally show no clear preference.

[30] Unlike all other shapes, the sine shapes exhibit phase shifts with changing timescale. This is particularly evident for the temperature shapes in stable conditions (Figure 8). The phase angle between the averaged w and T is π at scales below 2 min. At the two-min scale, w and T begin to drift out of phase and finally reach approximately quadrature at 5 min and beyond. According to linear theory, the internal gravity waves do not transport heat, i.e. they are characterized by the $\pi/2$ phase shift between w and T. On the other hand, the turbulence and Kelvin-Helmholtz instabilities have, on average, near 0 or π phase angle between w and T [e.g., *Rees et al.*, 2000]. Therefore, the relative proportion of gravity waves in the stable boundary layer seems to increase with timescale up to 5 min, and they dominate the w-T phase relationship for larger scales. This agrees well with the expected range of periods of atmospheric internal gravity waves [e.g., *Rees et al.*, 2000]. Below 2 min, the dominant sine-like shapes are related to either turbulent eddies or Kelvin-Helmholtz instabilities. The scale range between 1 and 5 min is then an overlap zone with mixed gravity waves and turbulence, and the prevalence of each probably depends on stability and wind speed.

4. Conclusion

[31] Extracting predefined shapes using simple linear correlation enabled a study of basic properties of different features in atmospheric boundary-layer time series. One year of high-frequency data were examined to construct the scale dependence of different shapes and their relationships to stability from timescales of 3 s to 2 h. The previously known decrease of energy at scales larger than turbulence scales, sometimes posed in terms of the mesoscale gap, is evident from the minima in the frequency of occurrence of shapes and depends on the thermodynamical stability in accordance with previous wisdom. However, the ratio of frequencies of occurrence of different shapes is surprisingly independent of timescale and seems to depend only on the variable that is examined. This yields a hypothesis that similar results might be obtained for other unrelated data sets, as these fundamental shapes are the building blocks of a wide range of different time series.

[32] The shapes captured from the temperature time series are "sharper" than those from the wind speed time series for all timescales. This might be related to pressure fluctuations and shear instability that act to smooth large momentum gradients. Furthermore, this finding is in broad agreement with the results from laboratory and numerical studies of scalar turbulence, where scalar intermittency, which is associated with steep-edged shapes, is not necessarily related to steeper shapes in the velocity field. The behavior of sharp edges of shapes revealed by the shape analysis suggests that these sharp features are forced by downward motions. This tendency becomes less obvious with increasing scale, which is consistent with weakening of vertical motions at larger scales. Sharp changes of wind speed at smaller and intermediate scales generally correspond to horizontal convergence (micro-frontogenesis) rather than divergence.

[33] The sine shapes are characterized by different phase relationships between variables for different scales, particularly for stable conditions. For scales less than two minutes, the phase angle between w and T is π, indicating active heat transport by these motions, most probably turbulent eddies and Kelvin-Helmholtz instability. For scales larger than two minutes, the phase angle is approximately $\pi/2$, indicating the dominance of internal gravity waves and hence the lack of heat transport, which is in agreement with the expected timescales of gravity waves in the atmosphere.

[34] These results clearly indicate that the physics of the processes that are responsible for generation of the time series shapes significantly changes with scale. However, the geometry of the structures is nearly independent of timescale.

[35] Ramp-cliff and cliff-ramp shapes are shown to have almost the same frequency of occurrence at all scales. However, the ramp-cliff patterns with $\partial T/\partial t < 0$ dominate the heat flux at smaller scales in unstable conditions, which is in agreement with the usual understanding. Although previous

turbulence studies showed that the ramp-cliff patterns with negative $\partial/\partial t$ (as defined here) are ubiquitous in turbulent fluids, an open question remains about what generates these shapes at different scales in the atmosphere. Also, the generation mechanisms for other ramp shapes are still unknown. Further understanding can be obtained from field experiments that include spatial networks of turbulence measurements that extend over several scales. This would enable better understanding of physical properties and spatial structure of individual shapes and their relation to the signals in time domain.

[36] **Acknowledgments.** The Kutina data were kindly provided by the Department of Geophysics, University of Zagreb. We particularly thank Zvjezdana Bencetić Klaić, Branko Grisogono and Željko Večenaj for support and assistance with the data collection. Three anonymous reviewers are gratefully acknowledged for their constructive comments and suggestions. This study was initiated during the first author's visit to Oregon State University sponsored by a Fulbright scholarship. The work was partially supported by the project AQCT, funded by the Croatian Ministry of Science, Education and Sport. L. Mahrt is supported by grant AGS-1115011 from the National Sciences Foundation.

References

Acevedo, O. C., O. L. L. Moraes, G. A. Degrazia, and L. E. Medeiros (2006), Intermittency and the exchange of scalars in the nocturnal surface layer, *Boundary Layer Meteorol.*, *119*, 41–55.

Anscombe, F. J. (1973), Graphs in statistical analysis, *Am. Stat.*, *27*, 17–21.

Antonia, R. A., A. J. Chambers, C. A. Friehe, and C. W. Van Atta (1979), Temperature ramps in the atmospheric surface layer, *J. Atmos. Sci.*, *36*, 99–108.

Armi, L., and P. Flament (1985), Cautionary remarks on the spectral interpretation of turbulent flows, *J. Geophys. Res.*, *90*, 11,779–11,782.

Barthlott, C., P. Drobinski, C. Fesquet, T. Dubos, and C. Pietras (2007), Long-term study of coherent structures in the atmospheric surface layer, *Boundary Layer Meteorol*, *125*, 1–24.

Basu, S., F. Porté-Agel, E. Foufoula-Georgiou, J. Vinuesa, and M. Pahlow (2006), Revisiting the local scaling hypothesis in stably stratified atmospheric boundary-layer turbulence: An integration of field and laboratory measurements with large-eddy simulations, *Boundary Layer Meteorol.*, *119*, 473–500.

Belušić, D., and L. Mahrt (2008), Estimation of length scales from mesoscale networks, *Tellus, Ser. A*, *60*, 706–715.

Campanharo, A. S. L. O., F. M. Ramos, E. E. N. Macau, R. R. Rosa, M. J. A. Bolzan, and L. D. A. Sá (2008), Searching chaos and coherent structures in the atmospheric turbulence above the Amazon forest, *Philos. Trans. R. Soc. A*, *366*, 579–589.

Cava, D., U. Giostra, M. Siqueira, and G. Katul (2004), Organised motion and radiative perturbations in the nocturnal canopy sublayer above an even-aged pine forest, *Boundary Layer Meteorol.*, *12*, 129–157.

Finnigan, J. (2000), Turbulence in plant canopies, *Annu. Rev. Fluid Mech.*, *32*, 519–571.

Gao, W., R. H. Shaw, and R. T. Paw U (1989), Observation of organized structure in turbulent flow within and above a forest canopy, *Boundary Layer Meteorol.*, *47*, 349–377.

Gibson, C. H., C. A. Friehe, and S. O. McConnell (1977), Structure of sheared turbulent fields, *Phys. Fluids*, *20*, S156–S167.

Holzer, M., and E. D. Siggia (1994), Turbulent mixing of a passive scalar, *Phys. Fluids*, *6*, 1820–1837.

Hunt, J. C. R., I. Eames, J. Westerweel, P. A. Davidson, S. Voropayev, J. Fernando, and M. Braza (2010), Thin shear layers—The key to turbulence structure?, *J. Hydrol. Environ. Res.*, *4*, 75–82.

Krusche, N., and A. P. De Oliveira (2004), Characterization of coherent structures in the atmospheric surface layer, *Boundary Layer Meteorol.*, *110*, 191–211.

Mahrt, L. (1991), Eddy asymmetry in the sheared heated boundary layer, *J. Atmos. Sci.*, *48*, 472–492.

Mahrt, L. (2010a), Common microfronts and other solitary events in the nocturnal boundary layer, *Q. J. R. Meteorol. Soc.*, *136*, 1712–1722.

Mahrt, L. (2010b), Computing turbulent fluxes near the surface: Needed improvements, *Agric. For. Meteorol.*, *150*, 501–509

Mahrt, L. (2011), The near-calm stable boundary layer, *Boundary Layer Meteorol.*, *140*, 343–360.

Mestayer, P. G., C. H. Gibson, M. F. Coantic, and A. S. Patel (1976), Local anisotropy in heated and cooled turbulent boundary layers, *Phys. Fluids*, *19*, 1279–1287.

Rees, J., J. Denholm-Price, J. King, and P. Anderson (2000), A climatological study of internal gravity waves in the atmospheric boundary layer overlying the Brunt Ice Self, Antarctica, *J. Atmos. Sci.*, *57*, 511–526.

Shraiman, B. I., and E. D. Siggia (2000), Scalar turbulence, *Nature*, *405*, 639–646.

Sun, J., et al. (2002), Intermittent turbulence associated with a density current passage in the stable boundary layer, *Boundary Layer Meteorol*, *105*, 199–219.

Sun, J., et al. (2004), Atmospheric disturbances that generate intermittent turbulence in nocturnal boundary layers, *Boundary Layer Meteorol.*, *110*, 255–279.

Taylor, R. J. (1958), Thermal structures in the lowest layers of the atmosphere, *Aust. J. Phys.*, *11*, 168–176.

van den Kroonenberg, A., and J. Bange (2007), Turbulent flux calculation in the polar stable boundary layer: Multiresolution flux decomposition and wavelet analysis, *J. Geophys. Res.*, *112*, D06112, doi:10.1029/2006JD007819.

Viana, S., C. Yagüe, and G. Maqueda (2009), Propagation and effects of a mesoscale gravity wave over a weakly-stratified nocturnal boundary layer during the SABLES2006 field campaign, *Boundary Layer Meteorol.*, *133*, 165–188.

Viana, S., E. Terradellas, and C. Yagüe (2010), Analysis of gravity waves generated at the top of a drainage flow, *J. Atmos. Sci.*, *67*, 3949–3966.

Vickers, D., and L. Mahrt (1997), Quality control and flux sampling problems for tower and aircraft data, *J. Atmos. Oceanic Technol.*, *14*, 512–526.

Vickers, D., and L. Mahrt (2006), Solution for flux contamination by mesoscale motions with very weak turbulence, *Boundary Layer Meteorol.*, *118*, 431–447.

Vindel, J. M., and C. Yagüe (2011), Intermittency of turbulence in the atmospheric boundary layer: Scaling exponents and stratification influence, *Boundary Layer Meteorol.*, *140*, 73–85.

Warhaft, Z. (2000), Passive scalars in turbulent flows, *Annu. Rev. Fluid Mech.*, *32*, 203–240.

Wesson, K. H., G. G. Katul, and M. Siqueira (2003), Quantifying organisation of atmospheric turbulent eddy motion using nonlinear time series analysis, *Boundary Layer Meteorol.*, *106*, 507–525.

Wilczak, J. M. (1984), Large-scale eddies in the unstably stratified atmospheric surface layer. Part I: Velocity and temperature structure, *J. Atmos. Sci.*, *41*, 3537–3550.

Wroblewski, D. E., O. R. Coté, J. M. Hacker, and R. J. Dobosy (2007), Cliff-ramp patterns and Kelvin-Helmholtz billows in stably stratified shear flow in the upper troposphere: Analysis of aircraft measurements, *J. Atmos. Sci.*, *64*, 2521–2539.